

# Selective impairment of circuits between prefrontal cortex glutamatergic neurons and basal forebrain cholinergic neurons in a tauopathy mouse model

Ping Zhong PhD, Qing Cao PhD, Zhen Yan PhD\*

Department of Physiology and Biophysics, Jacobs School of Medicine and Biomedical Sciences, State University of New York at Buffalo, Buffalo, NY 14203, United States

\*Corresponding author: State University of New York at Buffalo, 955 Main St., Room 3102, Buffalo, NY 14203, United States. Email: [zhenyan@buffalo.edu](mailto:zhenyan@buffalo.edu)

## Abstract

Alzheimer's disease (AD) is a prevalent neurodegenerative disorder linked to cognitive decline. To understand how specific neuronal circuits are impaired in AD, we have used optogenetic and electrophysiological approaches to reveal the functional changes between prefrontal cortex (PFC) and basal forebrain (BF), 2 key regions controlling cognitive processes, in a tauopathy mouse model. We found that the glutamatergic synaptic responses in BF cholinergic neurons from P301S Tau mice (6–8 months old) were markedly diminished. The attenuated long-range PFC to BF pathway in the AD model significantly increased the failure rate of action potential firing of BF cholinergic neurons triggered by optogenetic stimulations of glutamatergic terminals from PFC. In contrast, the projection from PFC to other regions, such as amygdala and striatum, was largely unaltered. On the other hand, optogenetic stimulation of cholinergic terminals from BF induced a persistent reduction of the excitability of PFC pyramidal neurons from Tau mice, instead of the transient reduction exhibited in wild-type mice. Taken together, these data have revealed a selective aberration of the pathway between PFC pyramidal neurons and BF cholinergic neurons in a tauopathy mouse model. This circuit deficit may underlie the loss of attention and executive function in AD.

**Key words:** Alzheimer's disease; prefrontal cortex; basal forebrain; optogenetics; patch-clamp recordings.

## Introduction

Cognitive decline in Alzheimer's disease (AD) is associated with multiple neuropathological features (Lawrence et al. 2017; Gan et al. 2018). The concept of neurodegeneration in AD has been expanded from the idea of general neuronal loss and astrogliosis to include earlier alterations such as synaptic and dendritic injury in specific brain circuits. To better understand the functional disturbances linked to AD-associated memory impairment, it is important to have the high-resolution mapping of cognitive circuits that go awry in AD. Optogenetic stimulation of specific pathways and ex vivo patch-clamp recording of synaptic responses (Gu and Yakel 2011; Yizhar et al. 2011; Chaudhury et al. 2013; Kim et al. 2013; Jiang et al. 2016; Zhong et al. 2020) provide the powerful tool to interrogate circuit changes in AD and the underlying synaptic mechanisms.

Prefrontal cortex (PFC) and basal forebrain (BF), 2 reciprocally connected key regions controlling cognitive processes (Gaykema et al. 1991; Woolf 1991; Chandler and Waterhouse 2012; Bloem et al. 2014), are degenerated at early stages of AD (Arnold et al. 1991; Teipel et al. 2005; Grothe et al. 2010; Grothe et al. 2012). PFC is composed of glutamatergic pyramidal projection neurons and GABAergic interneurons. It controls high-level executive functions by top-down governing of its innervated

regions, while it is also subject to bottom-up regulation by interconnected subcortical regions (Tomita et al. 1999; Buschman and Miller 2007; Comte et al. 2016; Yan and Rein 2021). BF is composed of cholinergic neurons and heterogeneous noncholinergic neurons that are distributed in a series of nuclei, including medial septal nucleus, diagonal band (DB) nuclei, preoptic nucleus, nucleus basalis (NB), and substantia innominata (SI) (Woolf 1991). Cholinergic neurons in NB and DB provide the predominant cholinergic projections to PFC (Mesulam et al. 1983; Woolf 1991; Bloem et al. 2014), which is directly engaged in attention and memory (Picciotto et al. 2012; Ballinger et al. 2016).

To find out whether the loss of cholinergic signaling is linked to cognitive impairment in neurodegenerative disorders as perceived before (Bartus et al. 1982; Grothe et al. 2010), we examined the alteration of long-range connections between PFC and BF in an AD model, the transgenic mouse carrying P301S mutation on human microtubule-associated protein Tau. P301S Tau mice reconstitute a variety of AD-related phenotypes, including tau filament abnormality, synapse loss, synaptic dysfunction, microglial activation, cognitive behavioral deficits, and neurodegeneration (Allen et al. 2002; Yoshiyama et al. 2007; Takeuchi et al. 2011; Onishi et al. 2014; Cao et al. 2020; Wang et al. 2021). To examine

Received: October 24, 2021. Revised: January 19, 2022. Accepted: January 20, 2022

© The Author(s) 2022. Published by Oxford University Press. All rights reserved. For permissions, please e-mail: [journals.permissions@oup.com](mailto:journals.permissions@oup.com)

the PFC to BF pathway, we injected ChR2 into PFC and recorded BF cholinergic neurons in response to optogenetic stimulation of glutamatergic terminals from PFC. On the other hand, to examine the BF to PFC pathway, we injected ChR2 into BF cholinergic neurons and recorded PFC pyramidal neurons in response to optogenetic stimulation of cholinergic terminals from BF. Our results have revealed a selective aberration of the pathway between PFC pyramidal neurons and BF cholinergic neurons in a tauopathy mouse model, which may contribute to the loss of attention and executive function in AD.

## Materials and methods

### Animals and surgery

All animal uses were approved by the IACUC of State University of New York at Buffalo. Wild-type (WT), Tau P301S transgenic mice (Yoshiyama et al. 2007) (Jackson Laboratory, 008169) and ChAT-IRES-Cre mice (Rossi et al. 2011) (Jackson Laboratory, 006410) were used in this study. AAV9.CAG.hChR2(H134R)-mCherry.WPRE.SV40 (ChR2) and pAAV-EF1a-double floxed-hChR2(H134R)-mCherry-WPRE-HGHpA (Cre-ChR2) were purchased from Penn Vector Core. Virus injection was conducted as previously described (Qin et al. 2018; Zhong et al. 2020; Rapanelli et al. 2021; Tan et al. 2021). Briefly, mice (~5 months old) were anesthetized with ketamine (95 mg/kg) and xylazine (5 mg/kg). After achieving deep anesthesia, using the stereotaxic apparatus (KoPF), we bilaterally injected ChR2 virus (1  $\mu$ L) into the medial PFC area (AP: 2.00 mm, ML:  $\pm$  0.5 mm, DV: -2 mm) or Cre-ChR2 virus (1  $\mu$ L) into the BF area (AP: -0.2 mm, ML:  $\pm$  1.5 mm, DV: -5.0 mm) through a Hamilton syringe (31 gauge). Injection speed was controlled using a microinjection pump (KD Scientific) (100 nL/min). The injection needle was left in place for 5 min following injection. Mice were allowed for viral expression for over 6 weeks before experimentation.

### Electrophysiological and optogenetic recordings

Mice were anesthetized with isoflurane and rapidly decapitated. Brains were quickly removed and submerged into the ice-cold sucrose solution (in mM: 234 sucrose, 4 MgSO<sub>4</sub>, 2.5 KCl, 1 NaH<sub>2</sub>PO<sub>4</sub>, 0.1 CaCl<sub>2</sub>, 15 HEPES, 11 glucose, pH 7.35). Coronal slices (300  $\mu$ m) containing BF regions including horizontal diagonal band (HDB) and SI were prepared on a vibratome (Leica VT1000s) in the ice-cold sucrose solution, then were transferred into artificial cerebrospinal fluid (ACSF) (in mM: 130 NaCl, 26 NaHCO<sub>3</sub>, 3 KCl, 5 MgCl<sub>2</sub>, 1.25 NaH<sub>2</sub>PO<sub>4</sub>, 1 CaCl<sub>2</sub>, 10 Glucose, pH 7.4, and 300 mOsm, oxygenated with 95% O<sub>2</sub> + 5% CO<sub>2</sub>), and kept at ~32 °C for 1 h and then at the room temperature (22–24 °C) for 1–4 h.

For recordings, 1 slice was positioned in a perfusion chamber attached to the fixed stage of an upright microscope (Olympus) and submerged in continuously

flowing oxygenated ACSF (external solution). Whole-cell patch-clamp experiments were performed with a Multi-clamp 700A amplifier and Digidata 1322A data acquisition system (Molecular Devices). Neurons were visualized with the infrared differential interference contrast video microscopy. Recording electrodes were pulled from borosilicate glass capillaries (1.5/0.86 mm OD/ID) with a micropipette puller (Sutter Instrument Co., model P-97). The resistance of patch electrode was 3–4.0 M $\Omega$ .

Optogenetic stimulation of ChR2-expressing neurons or terminals in brain slices was carried out via a microscope objective (Olympus LUMPlan FI/IR, 40X0.80w) using a UHP-Microscope-LED-460 system (Prizmatix) that provides >1 W collimated blue light (460 nm peak, 27 nm spectrum half width, 85% peak power at 450 nm). The blue light was triggered with TTL pulses programmed by the pClamp (Molecular Devices) data acquisition software and an on/off precision of about 0.1 ms was determined by the software-based acquisition rate. Single light pulses (width: 5 ms) or trains of light pulses (5 Hz, 4–5 pulse/train) were delivered during electrophysiological recordings.

Whole-cell voltage clamp was used to measure spontaneous excitatory postsynaptic current (sEPSC), EPSC evoked by electrical stimulation of neighboring neurons (eEPSC), and EPSC evoked by optogenetic stimulation of ChR2-expressing neurons or terminals (opto-EPSC). The internal solution contained (in mM): 130 Cs-methanesulfonate, 10 CsCl, 4 NaCl, 1 MgCl<sub>2</sub>, 5 EGTA, 10 HEPES, 4 Mg-ATP, 0.5 Na<sub>2</sub>GTP, and 10 Na-phosphocreatine. Whole-cell current clamp was used to record action potentials (APs) evoked by optogenetic stimulation of ChR2-expressing neurons or terminals (opto-AP) and synaptic-driven spontaneous action potential (sAP) firing. The internal solution contained (in mM): 20 KCl, 100 K-gluconate, 10 HEPES, 4 Mg-ATP, 0.5 Na<sub>2</sub>GTP, and 10 Na-phosphocreatine. For increasing neuronal activity in slices, a modified ACSF with lower magnesium (0.5 mM MgCl<sub>2</sub>) and higher potassium (3.5 mM KCl) was used as the external solution in the experiments for the recording of sEPSC, opto-AP, and sAP. To induce synaptic-driven sAP, a small (<50 pA) adjusting current (positive DC) was injected to elevate the membrane potential (inter-spike potential: -58 mV) (Maffei and Turrigiano 2008; Zhong and Yan 2016). APs evoked by injected currents were recorded in regular ACSF.

### Immunofluorescent staining

Six weeks after virus injection, mice were anesthetized and transcardially perfused as we previously described (Cao et al. 2020). Brain tissue was post-fixed in 4% paraformaldehyde and dehydrated with 30% sucrose for 2 consecutive days. Coronal sections (50  $\mu$ m) were cut with a vibrating microtome (Leica VT1000 S) and stored in cryoprotectant solution at -20 °C until ready to use. For illustrating the viral expression of ChR2(H134R)-mCherry in PFC, slices were blocked with PBS containing

5% goat serum (1 h, room temperature), followed by PBS washing and direct imaging with a Leica DMi8 fluorescence inverted microscope with Spiral function at 10× magnification. For labeling BF cholinergic neurons, slices were incubated with anti-ChAT (AB144P, 1:500, Millipore Sigma) at 4 °C overnight. For labeling PFC neurons, slices were incubated with anti-NeuN (1:500; Millipore, MAB377). After washing, slices were incubated with a fluorescent secondary antibody (A-11055, 1:1000, ThermoFisher Scientific) at room temp for 1 h. Images were acquired by using a Leica TCS SP8 confocal microscope.

### Data analysis

Data were acquired (sampling rate: 10 kHz, filtering frequency: 1 kHz) using the software Clampex 9.2 (Molecular Device). Data analyses were performed with the Clampfit software (Molecular Devices), Mini Analysis Program (Synaptosoft), and KaleidaGraph software. Statistical analysis was performed with Prism (GraphPad) and 2-tailed unpaired Student's *t*-test was used to determine the significance of differences between groups. All data are expressed as the mean ± SEM.

## Results

### Synaptic excitation in BF cholinergic neurons from P301S Tau mice is diminished

To find out whether cholinergic function in BF is impaired in the Tau model of AD, we performed whole-cell recordings of synaptic currents in cholinergic neurons at the HDB area of BF. Large oval-shaped neurons were identified to be BF cholinergic neurons, as we characterized previously (Gu et al. 2014). The sEPSC was first measured in the presence of a low-magnesium ACSF to enable the elevation of neuronal activity in slices (Maffei and Turrigiano 2008; Zhong and Yan 2016). As shown in Fig. 1A–C, sEPSC in BF cholinergic neurons from WT mice had numerous large high-frequency (bursting) events, while sEPSC in BF cholinergic neurons from P301S Tau mice had much smaller events and almost no bursting. When comparing sEPSC with a low threshold of 10 pA to include all events, a significant reduction of sEPSC amplitude, but not frequency, was found in BF cholinergic neurons from P301S Tau mice (Fig. 1D, WT:  $29.5 \pm 1.7$  pA,  $9.65 \pm 0.62$  Hz,  $n = 10$ , Tau:  $22.4 \pm 1.2$  pA,  $8.86 \pm 0.66$  Hz,  $n = 11$ , amp:  $t_{19} = 3.4$ ,  $P = 0.003$ , frequency:  $t_{19} = 0.9$ ,  $P = 0.39$ ). When only medium-sized (threshold: 25 pA) and large-sized (threshold: 45 pA) sEPSC events were selected, a significant reduction was found on both amplitude and frequency of sEPSC in BF cholinergic neurons from P301S Tau mice (Fig. 1D, 25 pA threshold, WT:  $48.6 \pm 3.1$  pA,  $3.73 \pm 0.38$  Hz,  $n = 10$ , Tau:  $37.3 \pm 1.9$  pA,  $2.08 \pm 0.24$  Hz,  $n = 11$ , amp:  $t_{19} = 3.2$ ,  $P = 0.005$ , frequency:  $t_{19} = 3.7$ ,  $P = 0.002$ ; 45 pA threshold, WT:  $67.2 \pm 3.3$  pA,  $1.68 \pm 0.17$  Hz,  $n = 10$ , Tau:  $55.9 \pm 2.0$  pA,  $0.64 \pm 0.13$  Hz,  $n = 11$ , amp:  $t_{19} = 3.0$ ,  $P = 0.007$ ; frequency:  $t_{19} = 4.9$ ,  $P < 0.001$ , *t*-test).

To further examine synaptic responses in BF cholinergic neurons, we measured EPSC evoked by electrical stimulation of neighboring glutamatergic inputs from local or long-range projections. AMPAR-EPSC was recorded at  $-70$  mV, and NMDAR-EPSC was recorded at  $+40$  mV (peak detected at 40 ms after electric stimulation when AMPAR inactivated) in the presence of bicuculline ( $10 \mu\text{M}$ ). Compared to WT mice, the amplitude of AMPAR-EPSC and NMDAR-EPSC was significantly smaller in BF cholinergic neurons from P301S Tau mice (Fig. 2A and B, AMPAR, WT:  $61.2 \pm 7.9$  pA,  $n = 10$ , Tau:  $42.1 \pm 3.9$  pA,  $n = 11$ ,  $t_{19} = 2.3$ ,  $P = 0.03$ ; NMDAR, WT:  $40.2 \pm 4.6$  pA,  $n = 10$ , Tau:  $27.7 \pm 3.6$  pA,  $n = 11$ ,  $t_{19} = 2.9$ ,  $P = 0.009$ , *t*-test), indicating the diminished glutamatergic transmission in these neurons.

### Optogenetic recordings reveal that PFC to BF cholinergic neurons pathway is selectively impaired in P301S Tau mice

BF cholinergic neurons are directly contacted by PFC afferents (Gaykema et al. 1991). The diminished synaptic responses in BF cholinergic neurons from Tau mice could be due to the reduced glutamatergic inputs from PFC. To test this, we first used optogenetic recordings to find out whether PFC provides an important excitatory projection to BF cholinergic neurons. The ChR2(H134R)-mCherry AAV was injected into PFC, and whole-cell patch-clamp recordings were performed on BF cholinergic neurons by light stimulation of glutamatergic terminals from PFC pyramidal projection neurons (Fig. 3A). Confocal images showed the expression of ChR2 in PFC neurons at the viral injection site (Fig. 3B). Moreover, ChR2 was transported to target regions innervated by PFC, including BF, and BF cholinergic neurons (ChAT+) also received rich projections from PFC (Fig. 3C).

BF is composed of heterogeneous types of neurons (Gritti et al. 2006). The glutamatergic inputs from PFC could directly activate BF cholinergic neurons or indirectly inactivate BF cholinergic neurons via feedforward inhibition by stimulating BF GABAergic inhibitory neurons (Fig. 3D). To test this, we recorded light-evoked EPSC (opto-EPSC, holding at  $-70$  mV) and IPSC (opto-IPSC, holding at 0 mV) in BF cholinergic neurons. As shown in Fig. 3E, AMPA receptor antagonist DNQX ( $50 \mu\text{M}$ ) blocked both opto-EPSC and opto-IPSC, while GABA<sub>A</sub>R antagonist bicuculline ( $10 \mu\text{M}$ ) only blocked opto-IPSC, indicating that opto-EPSC is mediated by AMPARs and opto-IPSC is mediated by GABA<sub>A</sub>Rs. These synaptic currents are both dependent on light stimulation of glutamatergic terminals from PFC, and opto-IPSC is likely generated via the disynaptic PFC to BF GABA interneuron to BF cholinergic neuron pathway. Light failed to induce any response in BF cholinergic neurons from mice without ChR2 virus injection (Fig. 3E), confirming that the optogenetic response was induced by stimulation of PFC to BF projections.

To examine the functional alteration of PFC to BF pathway in AD, we compared synaptic responses to optogenetic stimulation of PFC projections in BF

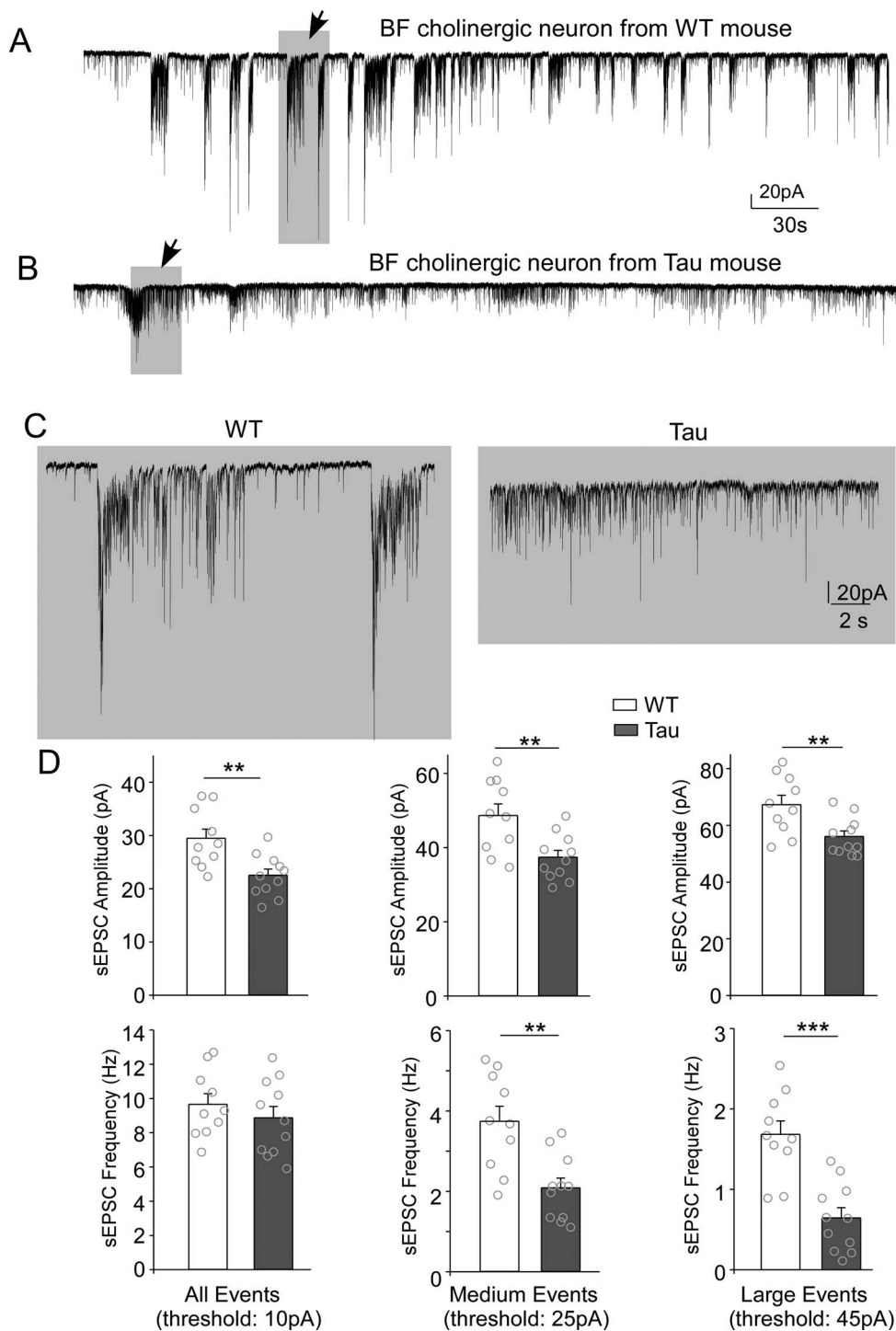


**Fig. 1.** BF cholinergic neurons from P301S Tau mice have the diminished baseline EPSCs. A, B) Representative sEPSC traces recorded in BF cholinergic neurons from 6-month-old WT and P301S Tau transgenic (Tau) mice. C) Expanded view of sEPSC traces from the selected regions in B (highlighted in gray). D) Bar graph showing the sEPSC amplitude and frequency in BF cholinergic neurons from WT versus Tau mice. All events (threshold: 10 pA), medium events (threshold: 25 pA), and large events (threshold: 45 pA) were compared. \*\* $P < 0.01$ ; \*\*\* $P < 0.001$ ,  $t$ -test.

cholinergic neurons from WT versus Tau mice. As shown in Fig. 4A and B, the amplitude of opto-EPSC and opto-IPSC was significantly reduced in BF cholinergic neurons from Tau mice (opto-EPSC, WT:  $121.2 \pm 17.2$  pA,  $n = 10$ ; Tau:  $71.5 \pm 9.1$  pA,  $n = 13$ ,  $t_{21} = 2.7$ ,  $P = 0.013$ ; opto-IPSC, WT:  $85.7 \pm 7.8$  pA,  $n = 10$ , Tau:  $57.9 \pm 7.6$  pA,  $n = 13$ ,  $t_{21} = 2.5$ ,  $P = 0.021$ ,  $t$ -test), suggesting the impairment of PFC  $\rightarrow$  BF circuit in AD.

PFC projects to many subcortical regions other than BF, such as basolateral amygdala (BLA) and striatum. To find out the specificity of the compromised PFC to BF pathway in AD, we also examined PFC to BLA and PFC to striatum pathways. BLA principal neurons can be directly activated by glutamatergic inputs from PFC and indirectly inactivated via feedforward inhibition from stimulated BLA inhibitory interneurons (Tan et al. 2021;

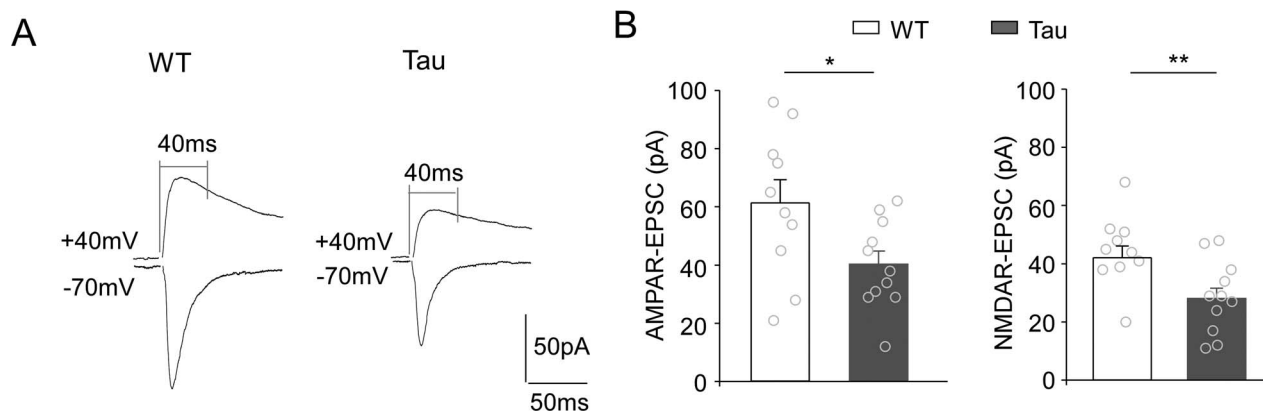


**Fig. 2.** BF cholinergic neurons from P301S Tau mice have the attenuated AMPAR- and NMDAR-mediated synaptic responses. A) Representative EPSC traces evoked by electrical stimuli in BF cholinergic neurons (held at  $-70$  mV for AMPAR-EPSC and  $+40$  mV for NMDAR-EPSC) from 6-month-old WT and Tau mice. B) Bar graph showing the AMPAR-EPSC and NMDAR-EPSC amplitudes in BF cholinergic neurons from WT versus Tau mice. \* $P < 0.05$ ; \*\* $P < 0.01$ , t-test.

Wang et al. 2021), so both opto-EPSC and opto-IPSC were detected in BLA principal neurons (Fig. 4C). However, no significant difference was found on the amplitude of opto-EPSC and opto-IPSC in BLA principal neurons from WT versus Tau mice (Fig. 4D, opto-EPSC, WT:  $131.2 \pm 10.2$  pA,  $n = 9$ ; Tau:  $128.8 \pm 9.8$  pA,  $n = 11$ ,  $t_{17} = 0.17$ ,  $P = 0.86$ ; opto-IPSC, WT:  $134.4 \pm 10.9$  pA,  $n = 9$ ; Tau:  $118.5 \pm 7.7$  pA,  $n = 11$ ,  $t_{17} = 1.9$ ,  $P = 0.07$ , t-test). In striatal medium spiny neurons (MSNs), opto-EPSC was detected, but opto-IPSC was not (Fig. 4E), suggesting the presence of excitatory projections from PFC to striatum and the lack of recurrent GABAergic connections among MSNs in striatum. No significant alteration was found on the amplitude of opto-EPSC in striatal medium spiny neurons from Tau mice (Fig. 4F, opto-EPSC, WT:  $72.4 \pm 7.6$  pA,  $n = 9$ ; Tau:  $64.6 \pm 4.9$  pA,  $n = 9$ ,  $t_{16} = 0.9$ ,  $P = 0.41$ , t-test).

Given the selective impairment of PFC to BF pathway in P301S Tau mice, we next examined its impact on the excitability of BF cholinergic neurons driven by PFC stimulation. APs evoked by optogenetic stimulations of glutamatergic terminals from PFC (opto-AP) were detected in BF cholinergic neurons (Fig. 5A). In contrast to the reliable triggering of opto-AP by light pulses in WT mice, a significantly higher failure rate of opto-AP was observed in P301S Tau mice (Fig. 5B, WT:  $14.3 \pm 7.4\%$ ,  $n = 7$ , Tau:  $62.5 \pm 6.7\%$ ,  $n = 8$ ,  $t_{13} = 4.8$ ,  $P < 0.001$ , t-test). Frequencies of APs evoked by injected currents were largely unchanged (Fig. 5C and D,  $n = 10$ /group,  $F_{1,16}(\text{genotype}) = 1.51$ ,  $P = 0.24$ , 2-way analysis of variance), indicating that the intrinsic firing properties are normal in BF cholinergic neurons from Tau mice. These data suggest that the impaired PFC to BF pathway causes functional deficiency of BF cholinergic neurons in AD.

### BF cholinergic neuron-mediated modulation of PFC pyramidal neuronal excitability is altered in P301S Tau mice

BF cholinergic neurons send extensive projections via their elaborate axon arbors to cortical targets including

PFC (Woolf 1991; Chandler and Waterhouse 2012; Bloem et al. 2014; Zaborszky et al. 2015). Next, we used optogenetic studies to find out whether the BF cholinergic to PFC pathway is also functionally altered in AD mice. ChAT-Cre mice, which have Cre expression in cholinergic neurons, were crossed with WT or Tau mice, and the Cre-dependent ChR2 virus, pAAV-EF1a-double floxed-hChR2(H134R)-mCherry-WPRE-HGHpA, was injected into BF of these mice. After 6 weeks of viral expression, we performed patch-clamp recordings of PFC pyramidal neurons that receive the cholinergic inputs from BF. Confocal images (Fig. 6A) showed the expression of ChR2 in BF cholinergic neurons (ChAT+) at the virus injection site. Moreover, ChR2 was transported to target regions innervated by BF cholinergic neurons, including PFC neurons (NeuN+).

Optogenetic stimulation of cholinergic terminals from BF, which can trigger ACh release within 100 ms of the light stimulus (Gritton et al. 2016), did not induce direct AP firing in PFC pyramidal neurons. So we examined the neuromodulatory effect of ACh (Picciotto et al. 2012; Jiang et al. 2016) by measuring its impact on the frequency of synaptic-driven, sAP in PFC (Zhong and Yan 2016). As shown in Fig. 6B and C, episodic stimulations of BF cholinergic inputs triggered a short-lived reduction of sAP frequencies in PFC pyramidal neurons from WT mice; however, a long-lasting reduction of sAP frequencies in response to repeated optogenetic stimulations of cholinergic terminals was observed in PFC pyramidal neurons from Tau mice. Thus, after 8–10 stimulations, Tau mice had a significantly lower sAP frequency than WT mice (WT:  $1.07 \pm 0.07$  Hz,  $n = 9$ , Tau:  $0.31 \pm 0.06$  Hz,  $n = 8$ ,  $t_{15} = 13.2$ ,  $P < 0.0001$ , t-test), suggesting that PFC pyramidal neurons are persistently suppressed by BF cholinergic inputs in AD.

### Discussion

One of the important and understudied questions in AD is how specific brain circuits are altered at the early

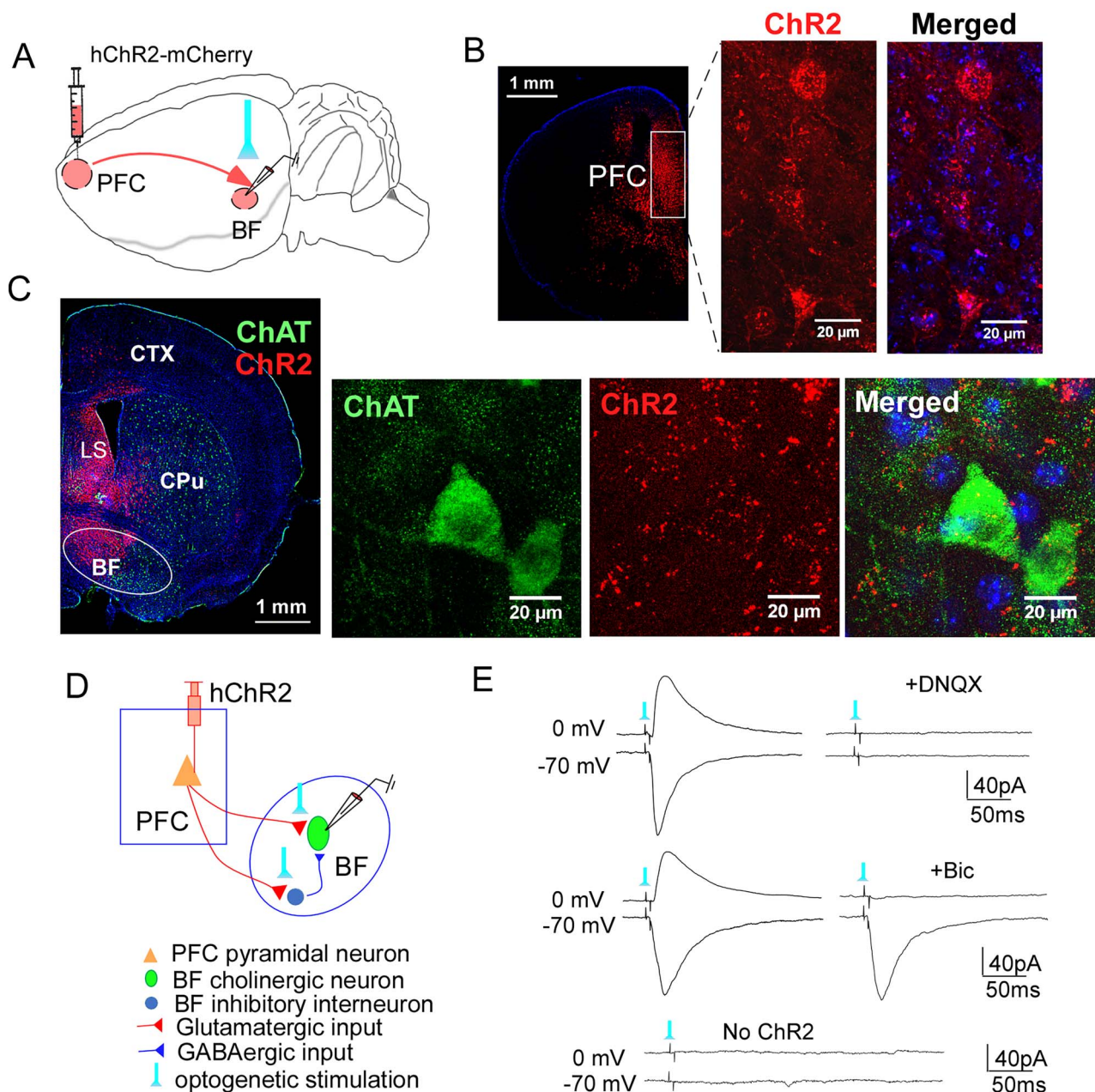


**Fig. 3.** Optogenetic recordings reveal that BF cholinergic neurons are functionally innervated by PFC. A–C) A diagram of the experimental setting (A) and confocal images showing the viral expression of ChR2(H134R)-mCherry in PFC (red, B, injection site) and ChR2-expressing terminals at the target regions including BF (red, C). Cholinergic neurons in BF are stained with anti-ChAT (green, C). Main brain regions on the image include: CTX (cortex), CPu (caudate putamen), LS (lateral septal), and BF. Blue: DAPI staining. The high-power images were from subregions of the low-power ones. D) Schematic diagram showing the inputs from PFC to BF cholinergic neurons directly and indirectly via the BF inhibitory interneuron. E) Representative traces of excitatory and inhibitory postsynaptic currents evoked by the blue light pulse (5-ms) stimulation (opto-EPSC, opto-IPSC) in BF cholinergic neurons. Opto-EPSC was recorded at  $-70$  mV, which was blocked by AMPAR antagonist DNQX ( $50 \mu\text{M}$ ). Opto-IPSC was recorded at  $0$  mV, which was blocked by GABA<sub>A</sub>R antagonist bicuculline ( $10 \mu\text{M}$ ). The response to light stimulation in a representative BF cholinergic neuron from a mouse without ChR2 virus injection is also shown.

stage, which leads to cognitive decline. Given the early compromise of PFC-mediated functions in AD, such as working memory, it is not surprising that PFC is one of the brain regions with a high vulnerability of degeneration in aging and AD (Raz et al. 1997; Salat et al. 2001). PFC controls high-level cognitive processes via interacting with its connected subcortical regions, including the BF cholinergic system (Tomita et al. 1999; Buschman and Miller 2007; Comte et al. 2016; Yan and Rein 2021). BF

atrophy is found in people with mild cognitive decline, and a widespread reduction of AChE expression and ACh receptors is found in patients with AD, implicating the critical role of cholinergic dysfunction in AD-related cognitive impairment (Teipel et al. 2005; Grothe et al. 2012; Ballinger et al. 2016).

Using P301S Tau mice, we first revealed the significant reduction of glutamatergic transmission in BF cholinergic neurons of the AD model. Large bursts of sEPSC

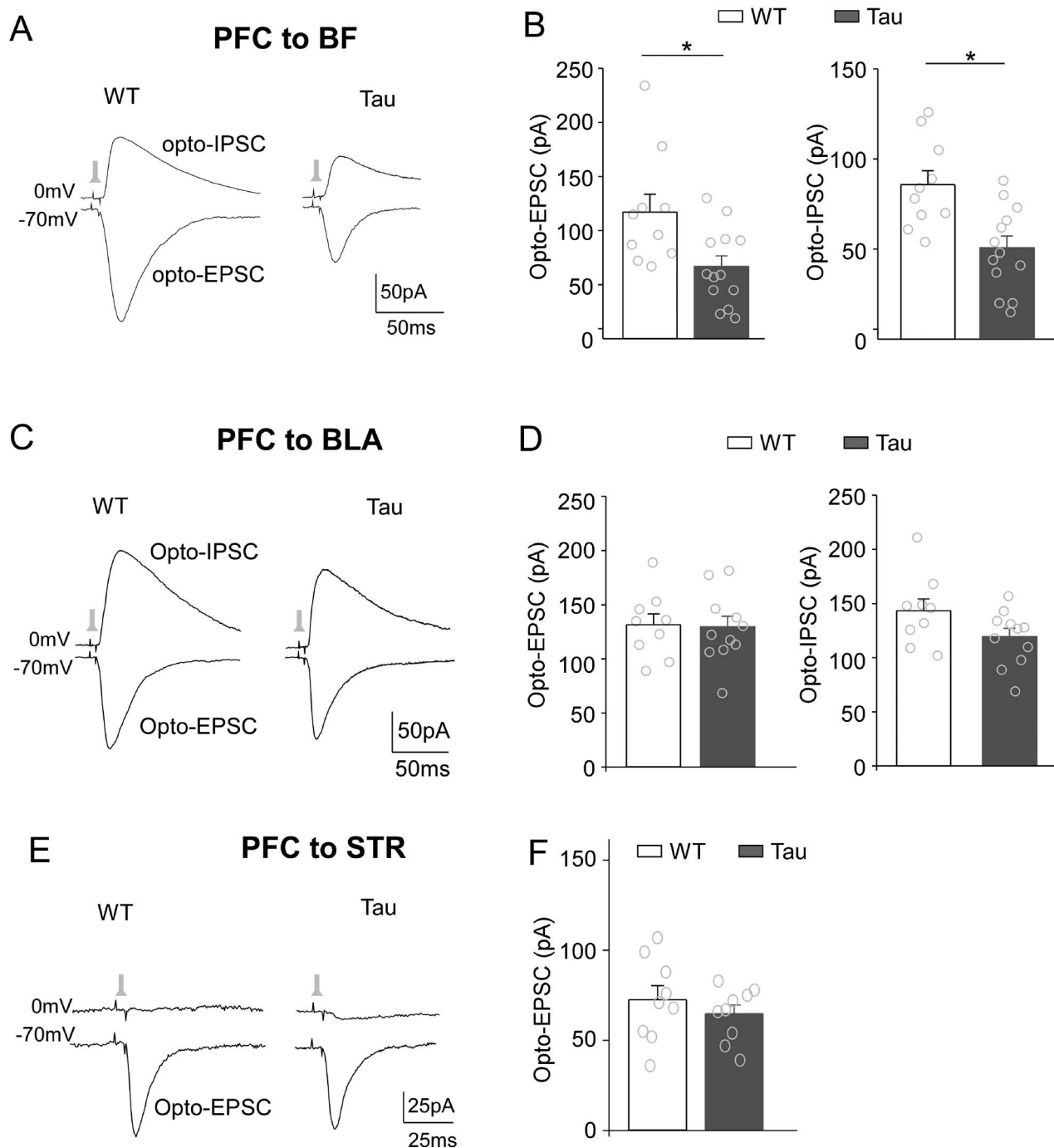


**Fig. 4.** Optogenetic recordings reveal that the PFC to BF pathway is selectively impaired in P301S Tau mice. A, C, E) Representative traces of opto-EPSC and opto-IPSC evoked by the blue light pulse stimulation in BF cholinergic neurons (A), BLA principal neurons (B), or striatal medium spiny neurons (C) from WT and Tau mice (~7–8 months old) with the injection of ChR2(H134R) in PFC. B, D, F) Bar graph showing the opto-EPSC and opto-IPSC amplitudes in BF cholinergic neurons (B), BLA principal neurons (D), or striatal medium spiny neurons (F) from WT versus Tau mice. \* $P < 0.05$ , t-test.

exhibited in BF cholinergic neurons of WT mice were not detected in Tau mice (Fig. 1). The reduced sEPSC amplitude and frequency (Fig. 1), as well as the diminished AMPAR- and NMDAR-mediated synaptic currents (Fig. 2), suggest that BF cholinergic neurons may have impaired glutamatergic inputs in AD.

Using optogenetic and electrophysiological approaches, we next revealed the functional changes in long-range connections from PFC glutamatergic neurons to BF

cholinergic neurons in the Tau AD model. BF cholinergic neurons are influenced by PFC inputs via direct glutamatergic excitation (monosynaptic) and indirect feedforward GABAergic inhibition (disynaptic) (Fig. 3). We find that BF cholinergic neurons in P301S Tau mice (~6 months old) receive the significantly diminished PFC inputs, as demonstrated by the reduced EPSC and IPSC evoked by optogenetic activation of PFC projections (Fig. 4). Consequently, BF cholinergic neurons in P301S

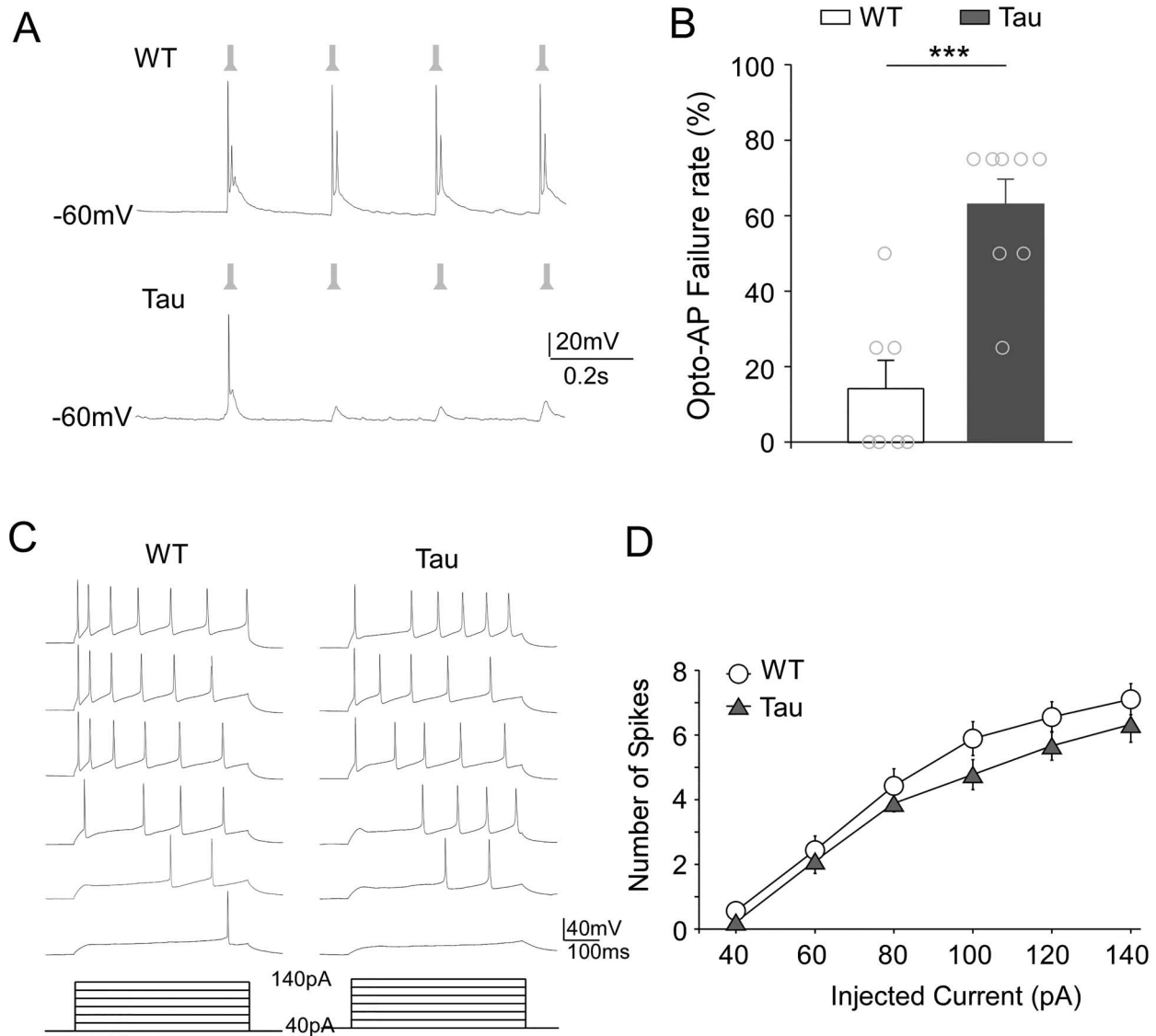


**Fig. 5.** BF cholinergic neurons have a higher failure rate of action potentials (APs) evoked by optogenetic stimulation of PFC to BF pathway in P301S Tau mice. A) Representative traces of APs in BF cholinergic neurons evoked by the blue light pulse stimulations (a train of four 5-ms pulses of 5 Hz) from WT and Tau mice with PFC injection of ChR2(H134R). B) Bar graph showing the failure rate of opto-APs in BF cholinergic neurons from WT versus Tau mice. \*\*\* $P < 0.001$ , t-test. C) Representative traces of APs evoked by injected currents in BF cholinergic neurons from WT and Tau mice. D) Plot of spike numbers in response to a series of injected currents in BF cholinergic neurons from WT and Tau mice.

Tau mice have the elevated failure rate of firing APs in response to the stimulation of PFC  $\rightarrow$  BF pathway (Fig. 5). In contrast to the attenuated PFC to BF pathway in the AD model, the projection from PFC to other regions, such as BLA and striatum, is not significantly altered (Fig. 4), suggesting the pathway specificity of the circuit changes in AD.

Molecular and cellular mechanisms underlying specific circuit alterations in AD await to be explored. We speculate that the disrupted microtubule stability resulting from the accumulation of hyperphosphorylated Tau in P301S mice interferes with the microtubule-based transport of cargos important for synaptic transmission in selective neuronal circuits, such as the long-range PFC to BF projections.

PFC receives extensive cholinergic inputs from BF (Woolf 1991; Chandler and Waterhouse 2012; Bloem et al. 2014; Zaborszky et al. 2015). Prior studies have found that stimulation of BF cholinergic inputs to release ACh in cortex triggers the excitation of cortical GABAergic interneurons via nicotinic receptors, leading to the feed-forward disinhibition of cortical pyramidal neurons (Gulledge and Stuart 2005; Arroyo et al. 2012). Subsequently, ACh depolarizes pyramidal neurons through muscarinic AChRs to increase their excitability (McCormick and Prince 1985). The impaired cholinergic excitation of PFC pyramidal neurons is exhibited in an AD model as a result of the excessive activation of calcium-activated hyperpolarizing conductance (Proulx et al. 2015). Here we have revealed that optogenetic

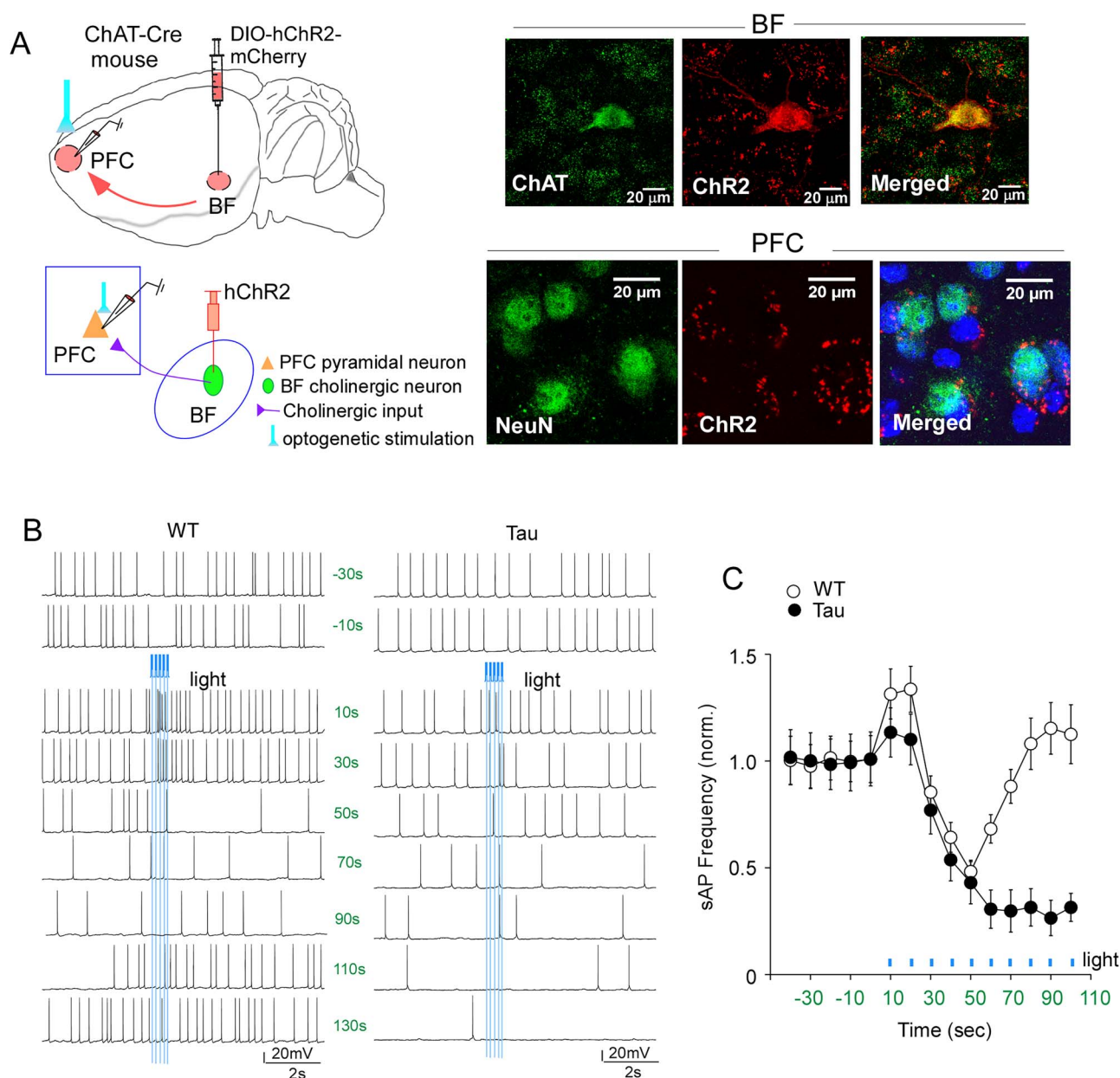


**Fig. 6.** Optogenetic stimulation of BF cholinergic neurons to PFC pathway induces a sustained reduction of spontaneous action potential (sAP) frequencies in PFC pyramidal neurons from P301S Tau mice. **A**) Left: Diagrams showing the experimental setting. DIO-ChR2-mCherry AAV was stereotactically injected into BF of ChAT-Cre mice, and recordings were performed in PFC pyramidal neurons. Right: Confocal images showing the expression of ChR2 (red) in BF cholinergic neurons (stained with anti-ChAT, green) at the virus injection site and ChR2-expressing terminals (red) in PFC neurons (stained with anti-NeuN, green) at the target region. Blue: DAPI staining. **B**) Synaptic-driven sAP traces in a representative PFC pyramidal neuron from a WT mouse (left) and a representative PFC pyramidal neuron from a Tau mouse (right) at various time points before and after episodic stimulations of ChR2-expressing terminals from BF cholinergic neurons with blue light pulses (5 trains of five 5-ms pulses of 5 Hz). **C**) Plot showing the averaged frequency of sAPs in PFC pyramidal neurons from WT and Tau mice at various time points before and after repeated optogenetic stimulations of inputs from BF cholinergic neurons. sAP frequencies of WT and Tau mice were normalized to 1 before optogenetic stimulations.

stimulation of cholinergic terminals from BF transiently reduces sAP frequencies in PFC pyramidal neurons from WT mice but induces a persistent reduction of sAP frequencies in those from P301S Tau mice (Fig. 6). The underlying mechanism for this neuromodulatory effect of synaptically released ACh is unclear. We speculate that the nicotinic inhibition of PFC pyramidal neurons, which is responsible for the early reduction of sAP frequency, is unchanged, but the delayed muscarinic activation of PFC pyramidal neurons, which is responsible for the later

increase of sAP frequency, is impaired in the AD model, leading to the altered temporal profile of ACh signaling.

Cholinergic circuits are at the center for normal executive function, and the loss of cholinergic signaling is strongly linked to cognitive decline (Ballinger et al. 2016). Our results have revealed a selective aberration of the pathway between PFC pyramidal neurons and BF cholinergic neurons in a tauopathy mouse model. The diminished PFC excitation of BF cholinergic neurons in AD reduces the release of ACh in widespread target regions,

including PFC. On the other hand, the sustained cholinergic inhibition of PFC pyramidal neurons in AD reduces PFC outputs to target regions, including BF. This vicious cycle impairs a central circuit for cognition, which may contribute to the loss of attention and memory in AD.

## Acknowledgments

We thank Xiaoqing Chen for her excellent technical support.

## Authors' contributions

PZ designed experiments, performed electrophysiological experiments, and analyzed data. QC performed immunohistochemical experiments. ZY designed experiments, supervised the project, and wrote the paper.

## Funding

This work was supported by grants from the National Institutes of Health (AG056060, AG064656, and AG067597) to ZY.

*Conflict of interest statement.* The authors report no competing financial or other interests.

## References

- Allen B, Ingram E, Takao M, Smith MJ, Jakes R, Virdee K, Yoshida H, Holzer M, Craxton M, Emson PC, et al. Abundant tau filaments and nonapoptotic neurodegeneration in transgenic mice expressing human P301S tau protein. *J Neurosci*. 2002;22:9340–9351.
- Arnold SE, Hyman BT, Flory J, Damasio AR, Van Hoesen GW. The topographical and neuroanatomical distribution of neurofibrillary tangles and neuritic plaques in the cerebral cortex of patients with Alzheimer's disease. *Cereb Cortex*. 1991;1:103–116.
- Arroyo S, Bennett C, Aziz D, Brown SP, Hestrin S. Prolonged disynaptic inhibition in the cortex mediated by slow, non- $\alpha 7$  nicotinic excitation of a specific subset of cortical interneurons. *J Neurosci*. 2012;32:3859–3864.
- Ballinger EC, Ananth M, Talmage DA, Role LW. Basal forebrain cholinergic circuits and Signaling in cognition and cognitive decline. *Neuron*. 2016;91:1199–1218.
- Bartus RT, Dean RL 3rd, Beer B, Lippa AS. The cholinergic hypothesis of geriatric memory dysfunction. *Science*. 1982;217:408–414.
- Bloem B, Schoppink L, Rotaru DC, Faiz A, Hendriks P, Mansvelter HD, van de Berg WD, Wouterlood FG. Topographic mapping between basal forebrain cholinergic neurons and the medial prefrontal cortex in mice. *J Neurosci*. 2014;34:16234–16246.
- Buschman TJ, Miller EK. Top-down versus bottom-up control of attention in the prefrontal and posterior parietal cortices. *Science*. 2007;315:1860–1862.
- Cao Q, Wang W, Williams JB, Yang F, Wang ZJ, Yan Z. Targeting histone K4 trimethylation for treatment of cognitive and synaptic deficits in mouse models of Alzheimer's disease. *Sci Adv*. 2020;6:eabc8096.
- Chandler D, Waterhouse BD. Evidence for broad versus segregated projections from cholinergic and noradrenergic nuclei to functionally and anatomically discrete subregions of prefrontal cortex. *Front Behav Neurosci*. 2012;6:20.
- Chaudhury D, Walsh JJ, Friedman AK, Juarez B, Ku SM, Koo JW, Ferguson D, Tsai HC, Pomeranz L, Christoffel DJ, et al. Rapid regulation of depression-related behaviours by control of midbrain dopamine neurons. *Nature*. 2013;493:532–536.
- Comte M, Schön D, Coull JT, Reynaud E, Khalfa S, Belzeaux R, Ibrahim EC, Guedj E, Blin O, Weinberger DR, et al. Dissociating bottom-up and top-down mechanisms in the cortico- limbic system during emotion processing. *Cereb Cortex*. 2016;26:144–155.
- Gan L, Cookson MR, Petrucelli L, La Spada AR. Converging pathways in neurodegeneration, from genetics to mechanisms. *Nat Neurosci*. 2018;21:1300–1309.
- Gaykema RP, van Weeghel R, Hersh LB, Luiten PG. Prefrontal cortical projections to the cholinergic neurons in the basal forebrain. *J Comp Neurol*. 1991;303:563–583.
- Gritti I, Henny P, Galloni F, Mainville L, Mariotti M, Jones BE. Stereological estimates of the basal forebrain cell population in the rat, including neurons containing choline acetyltransferase, glutamic acid decarboxylase or phosphate-activated glutaminase and colocalizing vesicular glutamate transporters. *Neuroscience*. 2006;143:1051–1064.
- Gritton HJ, Howe WM, Mallory CS, Hetrick VL, Berke JD, Sarter M. Cortical cholinergic signaling controls the detection of cues. *Proc Natl Acad Sci U S A*. 2016;113:E1089–E1097.
- Grothe M, Zaborszky L, Atienza M, Gil-Neciga E, Rodriguez-Romero R, Teipel SJ, Amunts K, Suarez-Gonzalez A, Cantero JL. Reduction of basal forebrain cholinergic system parallels cognitive impairment in patients at high risk of developing Alzheimer's disease. *Cereb Cortex*. 2010;20:1685–1695.
- Grothe M, Heinsen H, Teipel SJ. Atrophy of the cholinergic basal forebrain over the adult age range and in early stages of Alzheimer's disease. *Biol Psychiatry*. 2012;71:805–813.
- Gu Z, Yakel JL. Timing-dependent septal cholinergic induction of dynamic hippocampal synaptic plasticity. *Neuron*. 2011;71:155–165.
- Gu Z, Cheng J, Zhong P, Qin L, Liu W, Yan Z.  $A\beta$  selectively impairs mGluR7 modulation of NMDA signaling in basal forebrain cholinergic neurons: implication in Alzheimer's disease. *J Neurosci*. 2014;34:13614–13628.
- Gulledge AT, Stuart GJ. Cholinergic inhibition of neocortical pyramidal neurons. *J Neurosci*. 2005;25:10308–10320.
- Jiang L, Kundu S, Lederman JD, López-Hernández GY, Ballinger EC, Wang S, Talmage DA, Role LW. Cholinergic signaling controls conditioned fear behaviors and enhances plasticity of cortical-amygdala circuits. *Neuron*. 2016;90:1057–1070.
- Kim SY, Adhikari A, Lee SY, Marshel JH, Kim CK, Mallory CS, Lo M, Pak S, Mattis J, Lim BK, et al. Diverging neural pathways assemble a behavioural state from separable features in anxiety. *Nature*. 2013;496:219–223.
- Lawrence E, Vegvari C, Ower A, Hadjichrysanthou C, De Wolf F, Anderson RM. A systematic review of longitudinal studies which measure Alzheimer's disease biomarkers. *J Alzheimers Dis*. 2017;59:1359–1379.
- Maffei A, Turrigiano GG. Multiple modes of network homeostasis in visual cortical layer 2/3. *J Neurosci*. 2008;28:4377–4384.
- McCormick DA, Prince DA. Two types of muscarinic response to acetylcholine in mammalian cortical neurons. *Proc Natl Acad Sci U S A*. 1985;82:6344–6348.
- Mesulam MM, Mufson EJ, Levey AI, Wainer BH. Cholinergic innervation of cortex by the basal forebrain: cytochemistry and cortical connections of the septal area, diagonal band nuclei, nucleus basalis (substantia innominata), and hypothalamus in the rhesus monkey. *J Comp Neurol*. 1983;214:170–197.

- Onishi T, Matsumoto Y, Hattori M, Obayashi Y, Nakamura K, Yano T, Horiguchi T, Iwashita H. Early-onset cognitive deficits and axonal transport dysfunction in P301S mutant tau transgenic mice. *Neurosci Res.* 2014;80:76–85.
- Picciotto MR, Higley MJ, Mineur YS. Acetylcholine as a neuromodulator: cholinergic signaling shapes nervous system function and behavior. *Neuron.* 2012;76:116–129.
- Proulx É, Fraser P, McLaurin J, Lambe EK. Impaired cholinergic excitation of prefrontal attention circuitry in the TgCRND8 model of Alzheimer's disease. *J Neurosci.* 2015;35:12779–12791.
- Qin L, Ma K, Wang ZJ, Hu Z, Matas E, Wei J, Yan Z. Social deficits in Shank3-deficient mouse models of autism are rescued by histone deacetylase (HDAC) inhibition. *Nat Neurosci.* 2018;21:564–575.
- Rapanelli M, Tan T, Wang W, Wang X, Wang ZJ, Zhong P, Frick L, Qin L, Ma K, Qu J, et al. Behavioral, circuitry, and molecular aberrations by region-specific deficiency of the high-risk autism gene Cul3. *Mol Psychiatry.* 2021;26:1491–1504.
- Raz N, Gunning FM, Head D, Dupuis JH, McQuain J, Briggs SD, Loken WJ, Thornton AE, Acker JD. Selective aging of the human cerebral cortex observed in vivo: differential vulnerability of the prefrontal gray matter. *Cereb Cortex.* 1997;7:268–282.
- Rossi J, Balthasar N, Olson D, Scott M, Berglund E, Lee CE, Choi MJ, Lauzon D, Lowell BB, Elmquist JK. Melanocortin-4 receptors expressed by cholinergic neurons regulate energy balance and glucose homeostasis. *Cell Metab.* 2011;13:195–204.
- Salat DH, Kaye JA, Janowsky JS. Selective preservation and degeneration within the prefrontal cortex in aging and Alzheimer disease. *Arch Neurol.* 2001;58:1403–1408.
- Takeuchi H, Iba M, Inoue H, Higuchi M, Takao K, Tsukita K, Karatsu Y, Iwamoto Y, Miyakawa T, Suhara T, et al. P301S mutant human tau transgenic mice manifest early symptoms of human tauopathies with dementia and altered sensorimotor gating. *PLoS One.* 2011;6:e21050.
- Tan T, Wang W, Liu T, Zhong P, Conrow-Graham M, Tian X, Yan Z. Neural circuits and activity dynamics underlying sex-specific effects of chronic social isolation stress. *Cell Rep.* 2021;34:108874.
- Teipel SJ, Flatz WH, Heinsen H, Bokde AL, Schoenberg SO, Stöckel S, Dietrich O, Reiser MF, Möller HJ, Hampel H. Measurement of basal forebrain atrophy in Alzheimer's disease using MRI. *Brain.* 2005;128:2626–2644.
- Tomita H, Ohbayashi M, Nakahara K, Hasegawa I, Miyashita Y. Top-down signal from prefrontal cortex in executive control of memory retrieval. *Nature.* 1999;401:699–703.
- Wang W, Cao Q, Tan T, Yang F, Williams JB, Yan Z. Epigenetic treatment of behavioral and physiological deficits in a tauopathy mouse model. *Aging Cell.* 2021;20:e13456.
- Wolf NJ. Cholinergic systems in mammalian brain and spinal cord. *Prog Neurobiol.* 1991;37:475–524.
- Yan Z, Rein B. Mechanisms of synaptic transmission dysregulation in the prefrontal cortex: pathophysiological implications. *Mol Psychiatry.* 2021. <https://doi.org/10.1038/s41380-021-01092-3>.
- Yizhar O, Fenno LE, Prigge M, Schneider F, Davidson TJ, O'Shea DJ, Sohal VS, Goshen I, Finkelstein J, Paz JT, et al. Neocortical excitation/inhibition balance in information processing and social dysfunction. *Nature.* 2011;477:171–178.
- Yoshiyama Y, Higuchi M, Zhang B, Huang SM, Iwata N, Saido TC, Maeda J, Suhara T, Trojanowski JQ, Lee VM. Synapse loss and microglial activation precede tangles in a P301S tauopathy mouse model. *Neuron.* 2007;53:337–351.
- Zaborszky L, Csordas A, Mosca K, Kim J, Gielow MR, Vadasz C, Nadasdy Z. Neurons in the basal forebrain project to the cortex in a complex topographic organization that reflects corticocortical connectivity patterns: an experimental study based on retrograde tracing and 3D reconstruction. *Cereb Cortex.* 2015;25:118–137.
- Zhong P, Yan Z. Distinct physiological effects of dopamine D4 receptors on prefrontal cortical pyramidal neurons and fast-spiking interneurons. *Cereb Cortex.* 2016;26:180–191.
- Zhong P, Qin L, Yan Z. Dopamine differentially regulates response dynamics of prefrontal cortical principal neurons and interneurons to optogenetic stimulation of inputs from ventral tegmental area. *Cereb Cortex.* 2020;30:4402–4409.